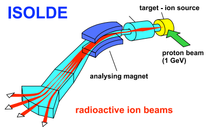

Magiske tal –
nu så magiske at de forsvinder

Karsten Riisager

IFA, AU

Kernekortet

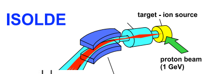

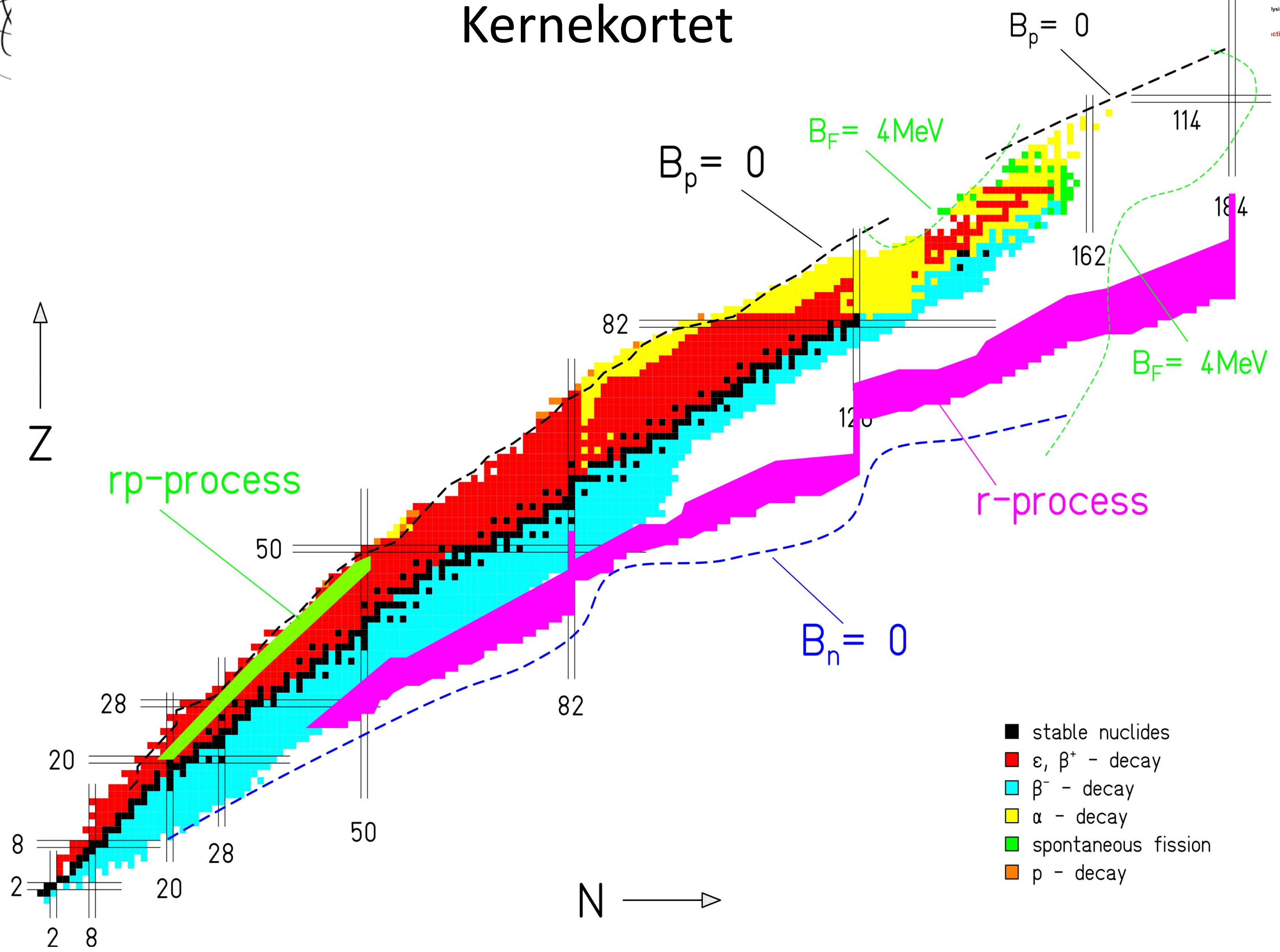

Skaller:

- Ekstra stabilitet
- Grundsten for strukturforklaringer
- Oprindelse i “niveau-bundter”

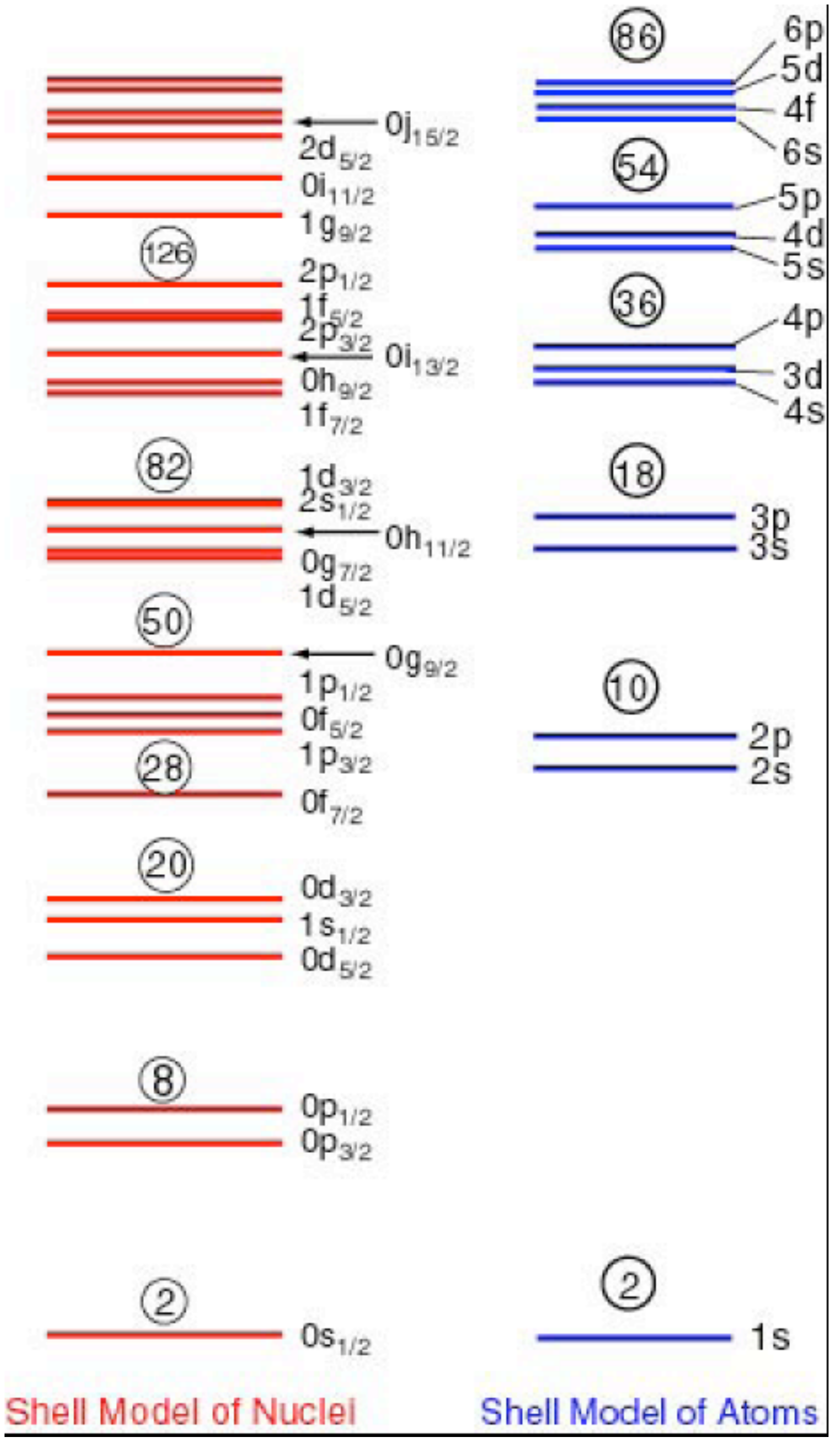

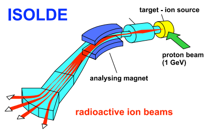

Kernetilstande ifølge skalmodellen

- Wood Saxon + L.S

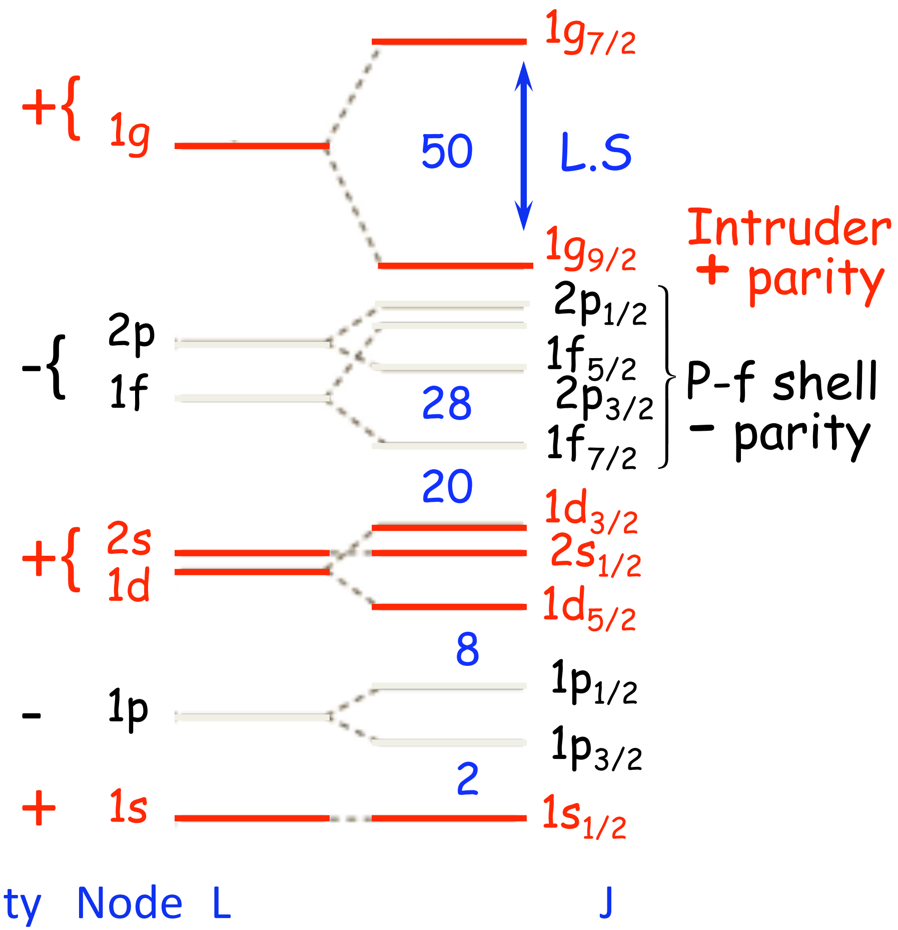

+{ $1g$

$1g_{7/2}$

50

L.S

$1g_{9/2}$

Intruder
+ parity

-{ $2p$ $1f$

$2p_{1/2}$

$1f_{5/2}$

$2p_{3/2}$

28

$1f_{7/2}$

P-f shell
- parity

20

+{ $2s$ $1d$

$1d_{3/2}$

$2s_{1/2}$

$1d_{5/2}$

8

- $1p$

$1p_{1/2}$

$1p_{3/2}$

2

+ $1s$

$1s_{1/2}$

Parity Node L J

Goeppert-Mayer

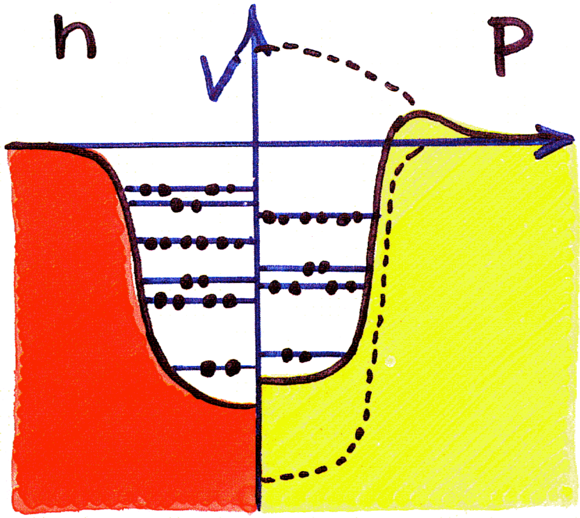

Nucleons in a self-consistent mean-field

Eksperimentelle skaller via systematik

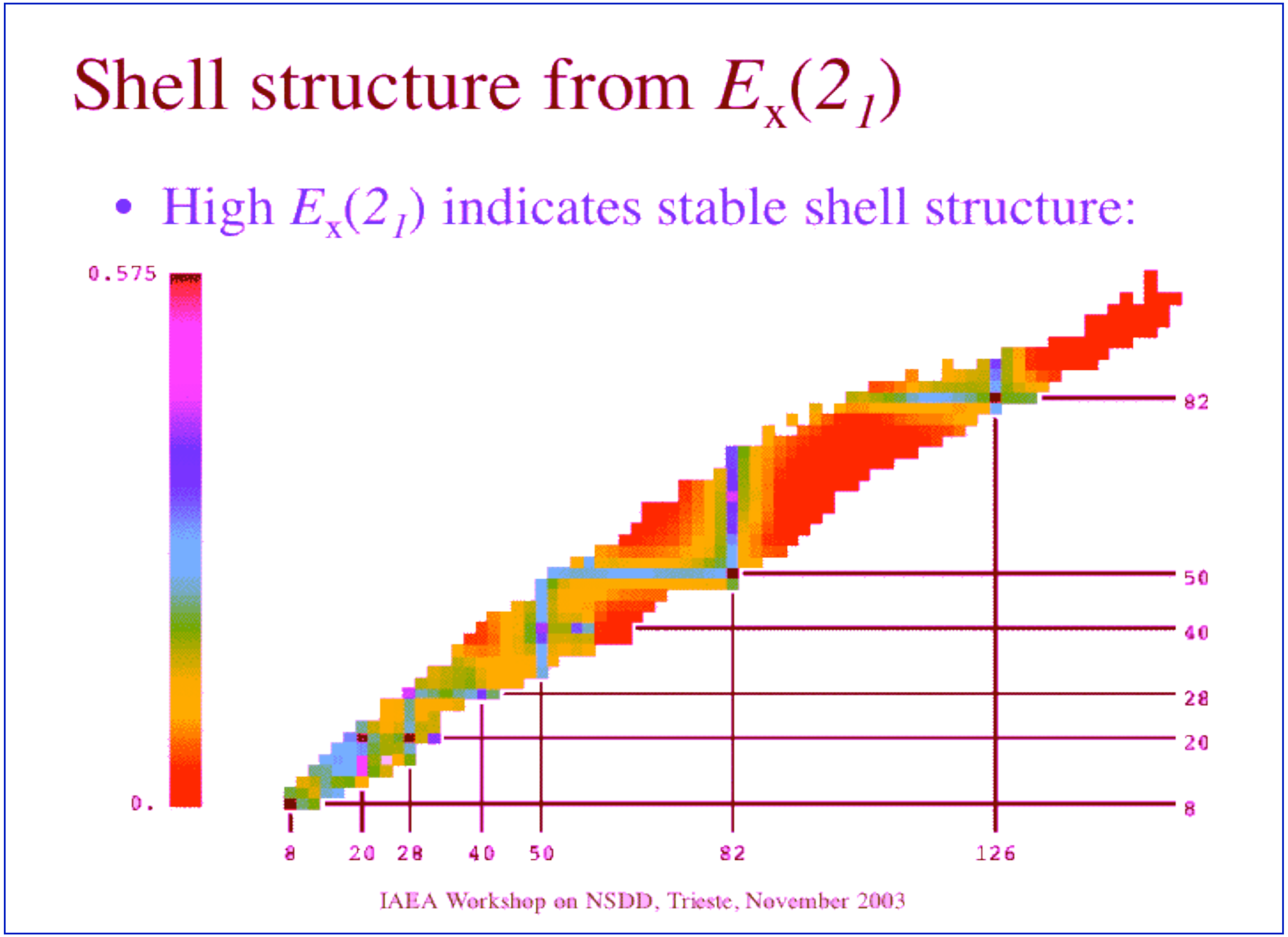

Shell structure from $E_x(2_1)$

- High $E_x(2_1)$ indicates stable shell structure:

IAEA Workshop on NSDD, Trieste, November 2003

Ændrede magiske tal…

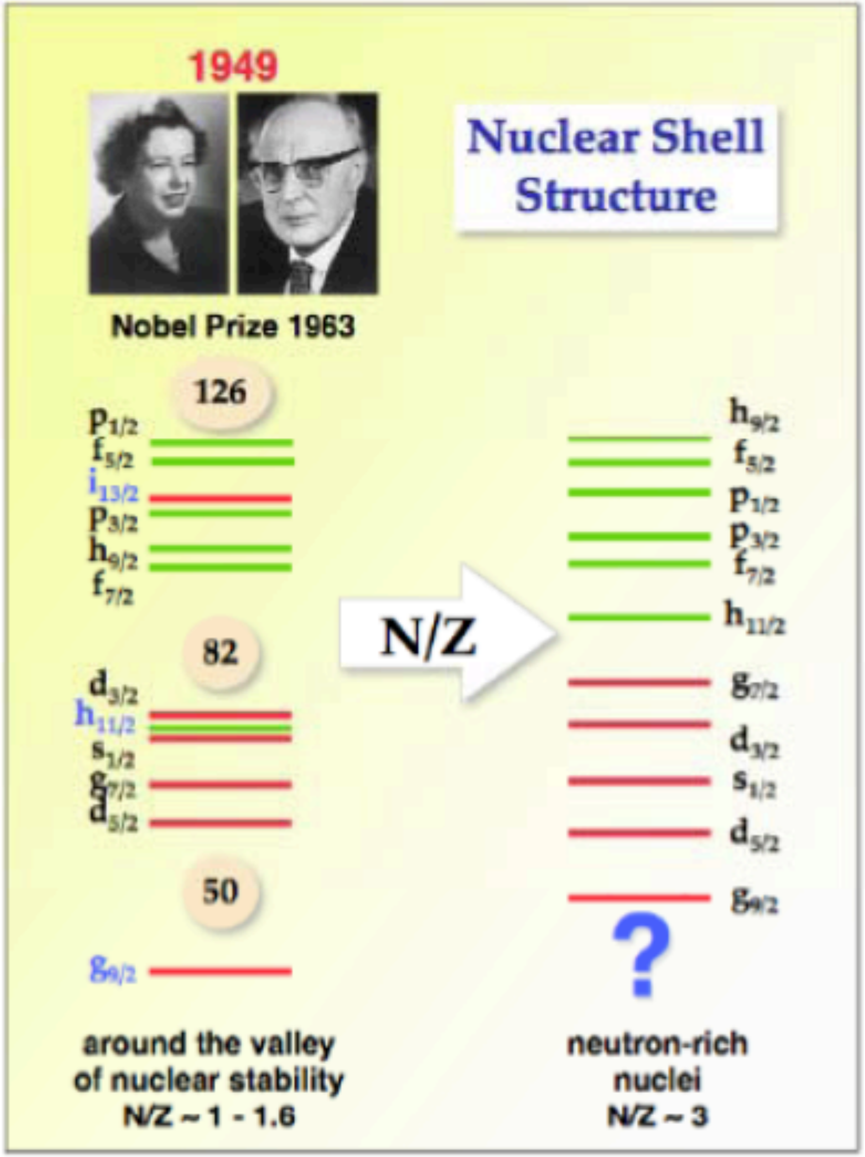

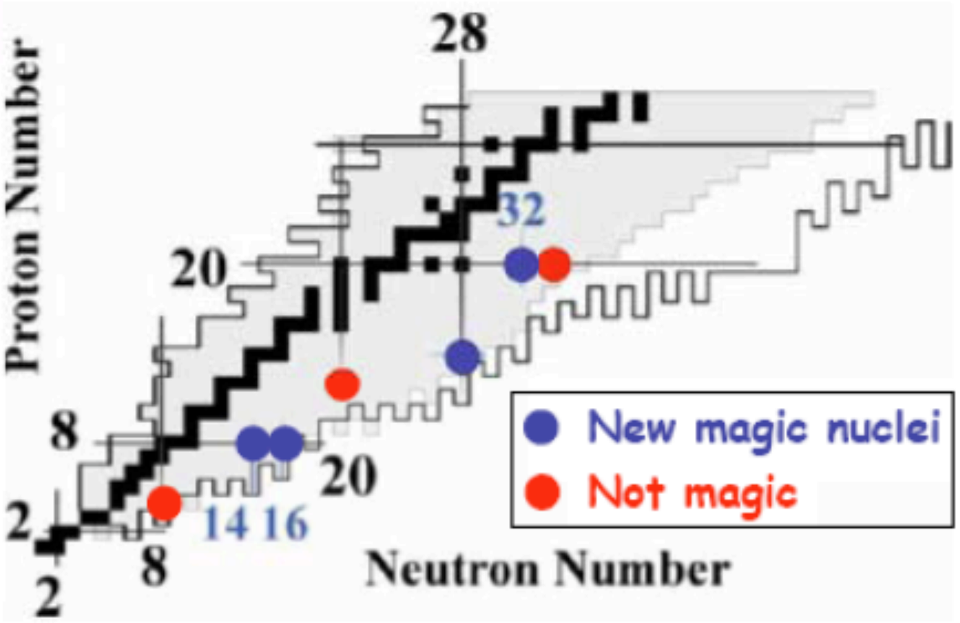

No shell closure for N=8 and 20 for drip-line nuclei; new shells at 14, 16, 32…

R. Casten

“Island of inversion”

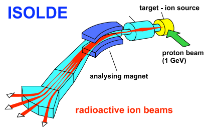

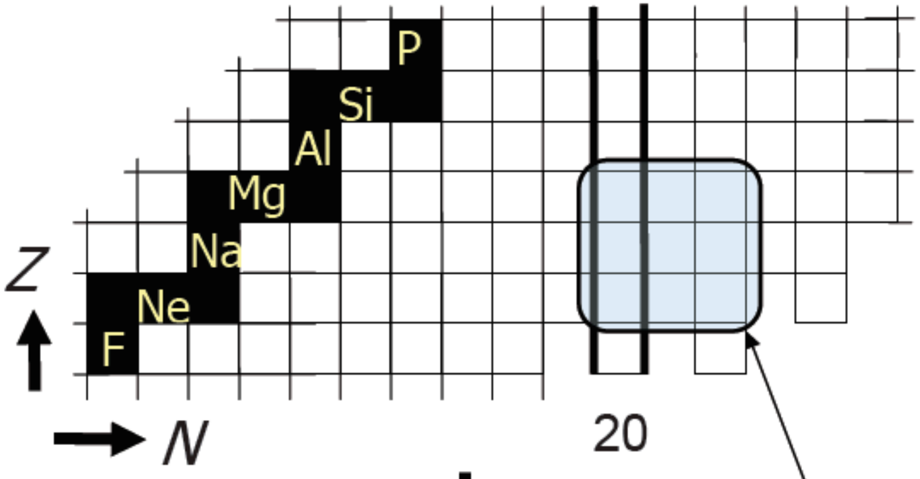

Island of Inversion

E.K. Warburton, J. A. Becker
and B. A. Brown, PRC**41**(1990)1147.

Normal *sd*-shell
configuration

0p0h, spherical

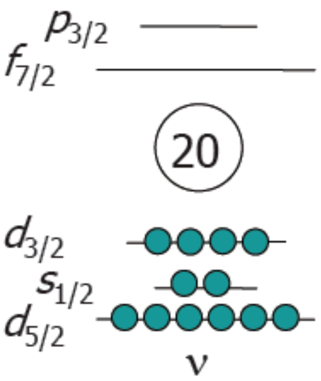

2p2h (intruder), deformed

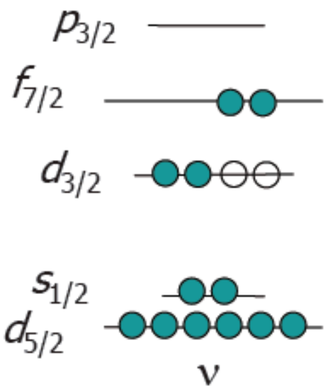

Monte Carlo shell model
sdpf model space: Na isotopes

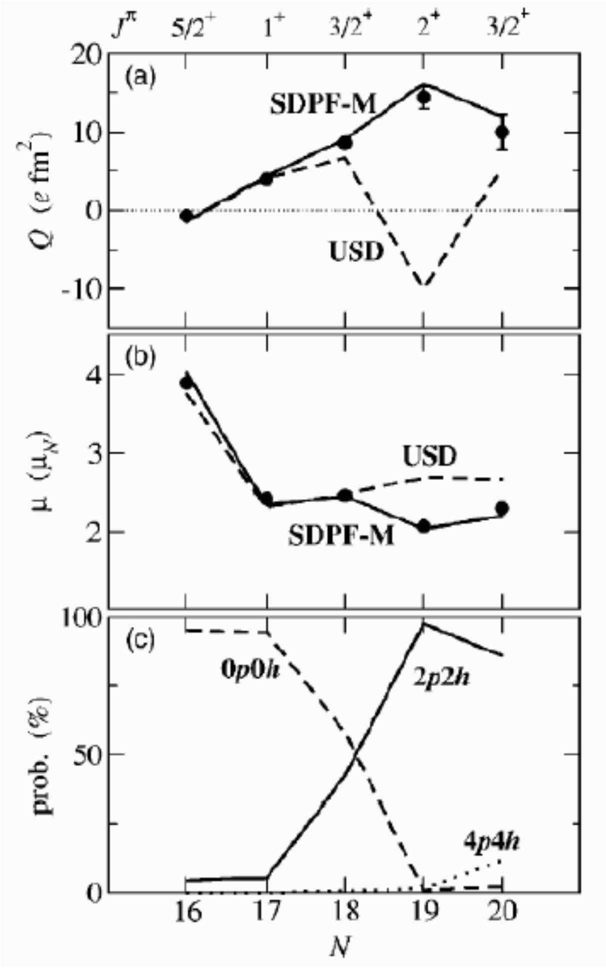

Y. Utsuno, *et al.*, Phys. Rev. C**70**(2004) 044307.

P. Reiter

Changing Magic Numbers

Magic closed-shell numbers (N or Z = 2,8,20,28,50,82 and 126) are well established for nuclei near the region of β-stability. They are predicted by the spherical shell model that approximates the nuclear potential by a self-consistent mean field as derived microscopically from Hartree-Fock Bogoliubov theory (see left part of the figure below which is drawn for a harmonic oscillator potential). The ordering of proton (neutron) energies will strongly depend on the filling of neutron (proton) orbitals through the self-energy Hartree-Fock correction based on the monopole part of the interaction.

When approaching the neutron-drip line, a more gradual decrease of the neutron average potential towards large radial values might occur. This can have drastic effects on the nuclear shell structure, even changing magic numbers (see right part of the figure below).

The monopole part of the effective force induces drastic changes in the single-particle energies resulting in changes in the magic numbers far from the line of stability. By studying, e.g., shifts in single-particle energies in light nuclei, it was shown that the neutron magic numbers at N=8 and N=20 can change into N=6 and N=16 for neutron-rich nuclei. As protons are added, i.e. moving towards the valley of stability, the strong attractive proton-neutron interaction brings the standard magic numbers back. This particular mechanism hints to an overall modification of standard values of closed shells for exotic nuclei.

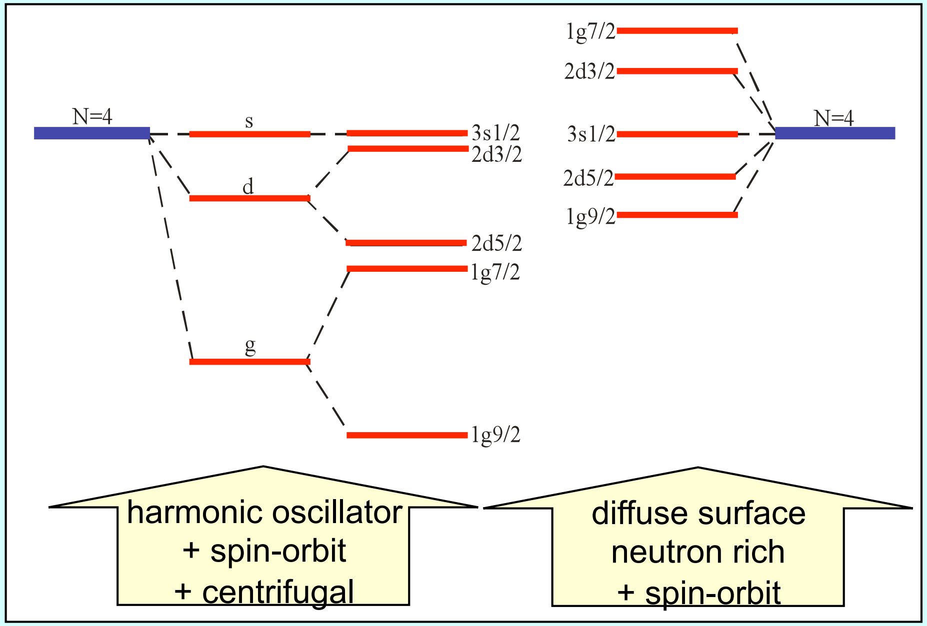

harmonic oscillator
+ spin-orbit
+ centrifugal

diffuse surface
neutron rich
+ spin-orbit

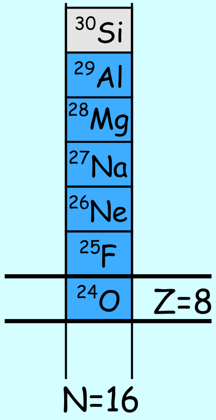

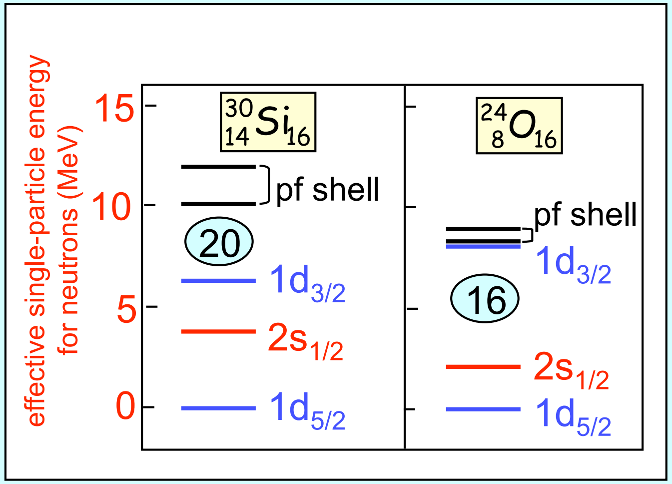

The figure compares the stable isotope ^{30}Si with the exotic nucleus ^{24}O. The former nucleus has 6 protons outside the closed Z=8 shell, while the latter has a closed proton-shell configuration. Due to the monopole part of the effective $\pi 1d_{5/2}-\nu 1d_{3/2}$ interaction, the well known N=20 gap is reduced and a new gap appears at N=16.

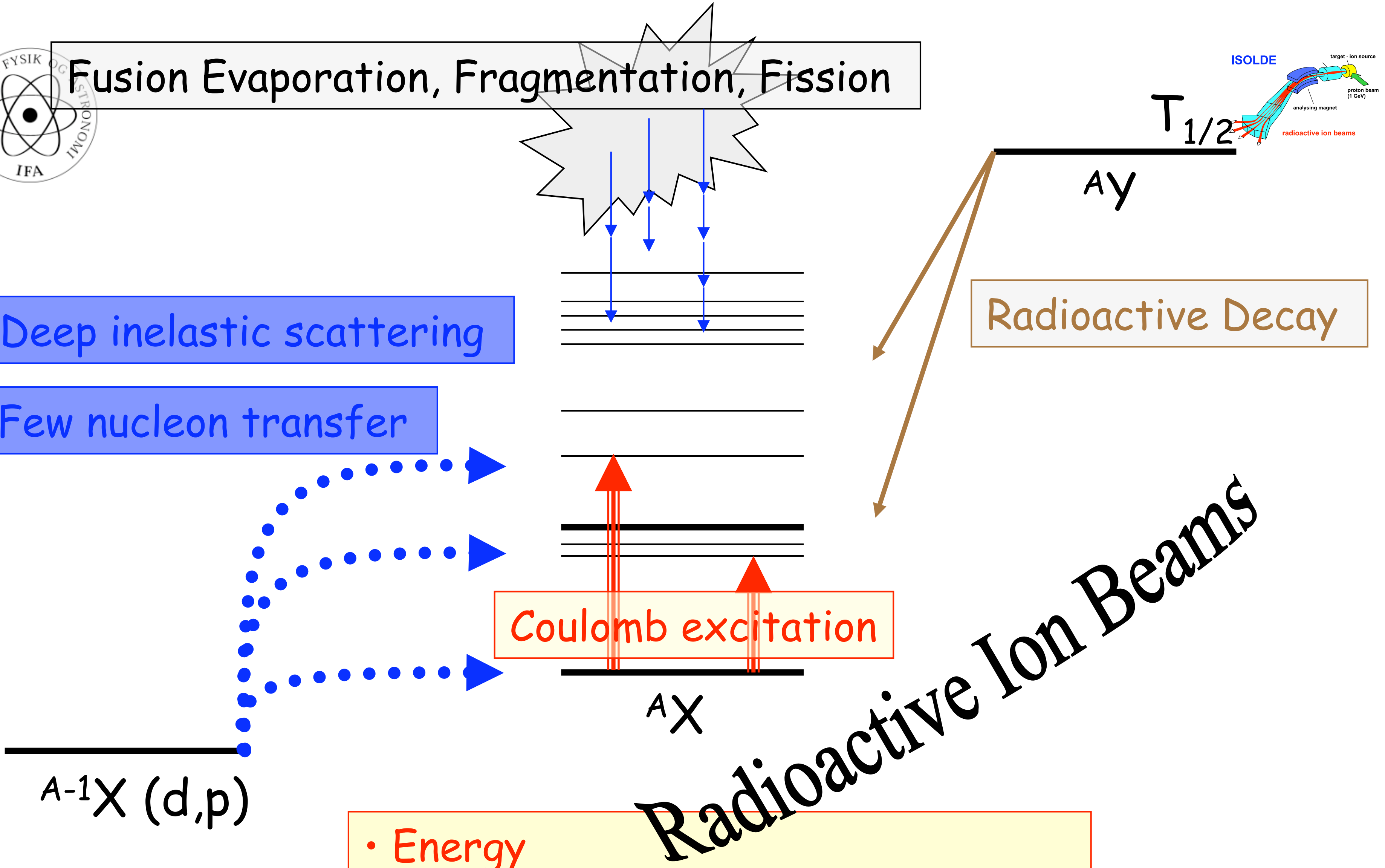

Fusion Evaporation, Fragmentation, Fission

Deep inelastic scattering

Few nucleon transfer

Coulomb excitation

Radioactive Decay

Radioactive Ion Beams

- Energy
- Spin and Parity
- Decay Strength Distributions
- **E.M.-**Transition Matrix Elements
- Spectroscopic Factors
- Shape and Moments

P. Van Duppen

To måder at lave radioactive beams:

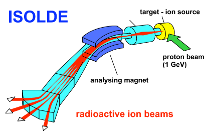

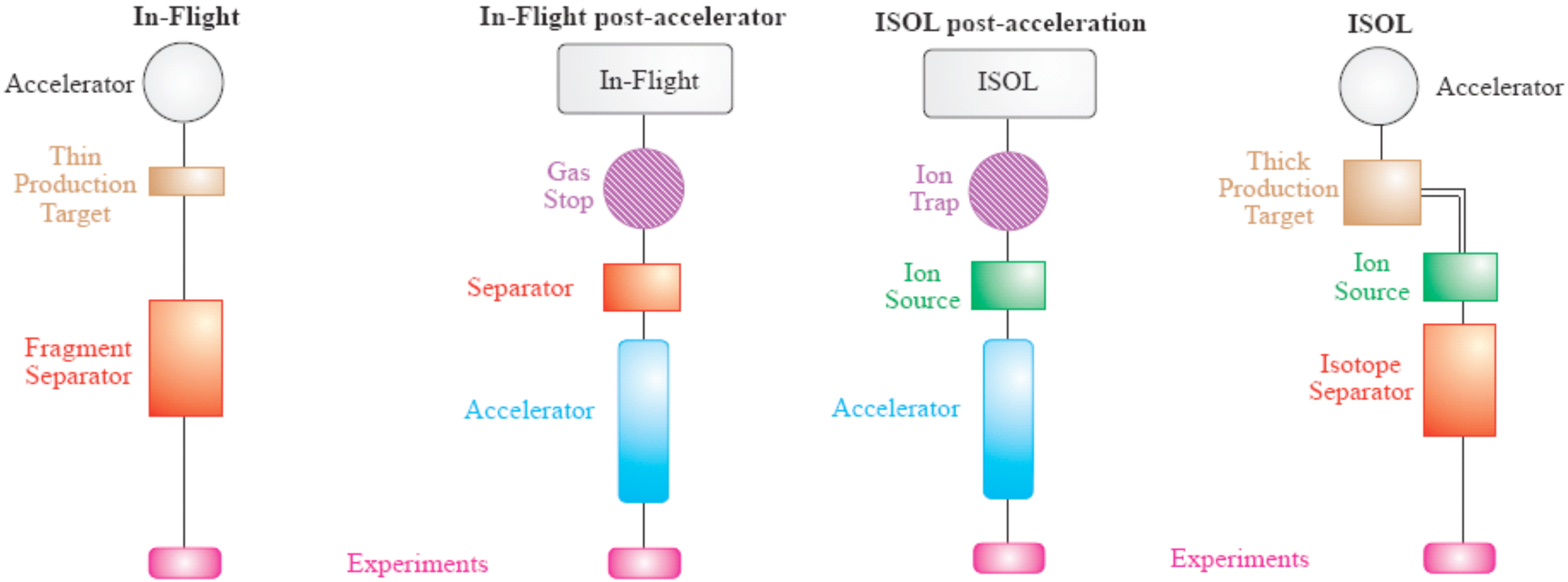

… to måder at post-accelerere

B. Jonson

CERN accelerator kompleks

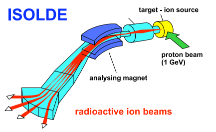

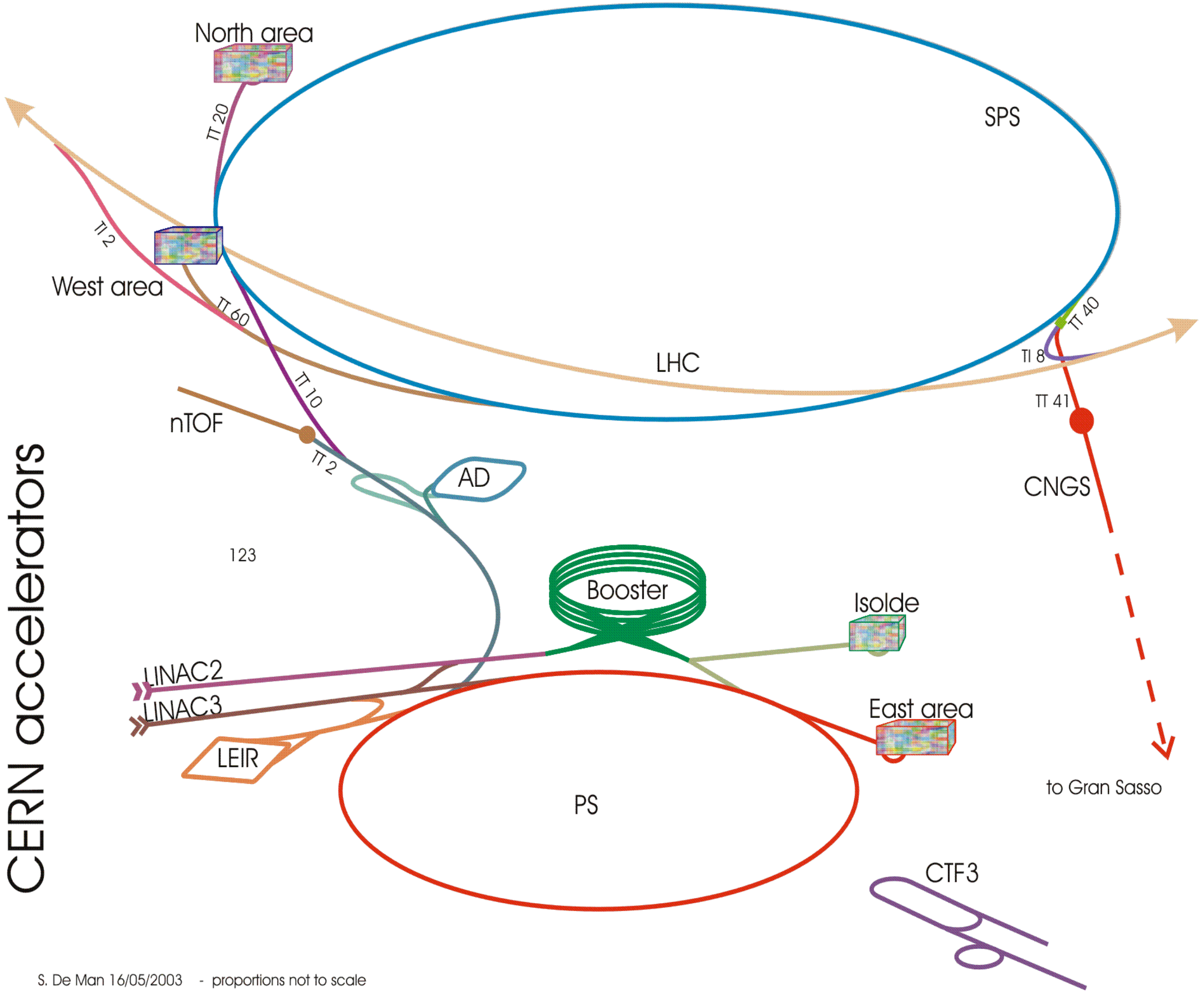

S. De Man 16/05/2003 - proportions not to scale

Targets

Produced via
- spallation, fragmentation or fission
- in foils, powders, liquids

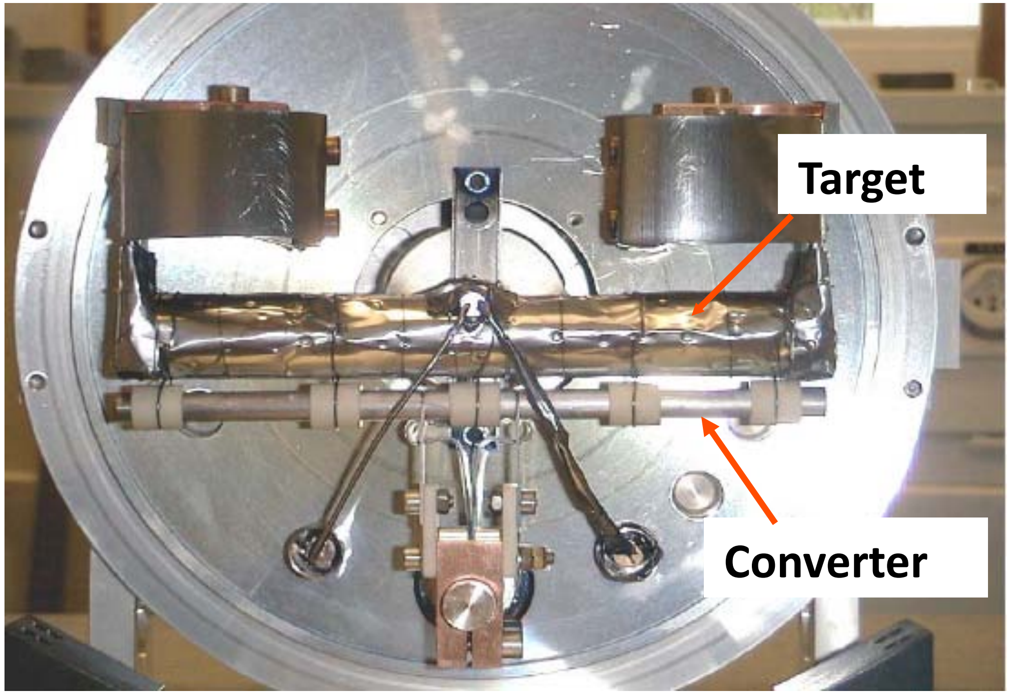

Converter Target

Standard

E. Siesling

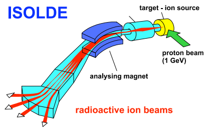

Ionkilde

Laser ionisering

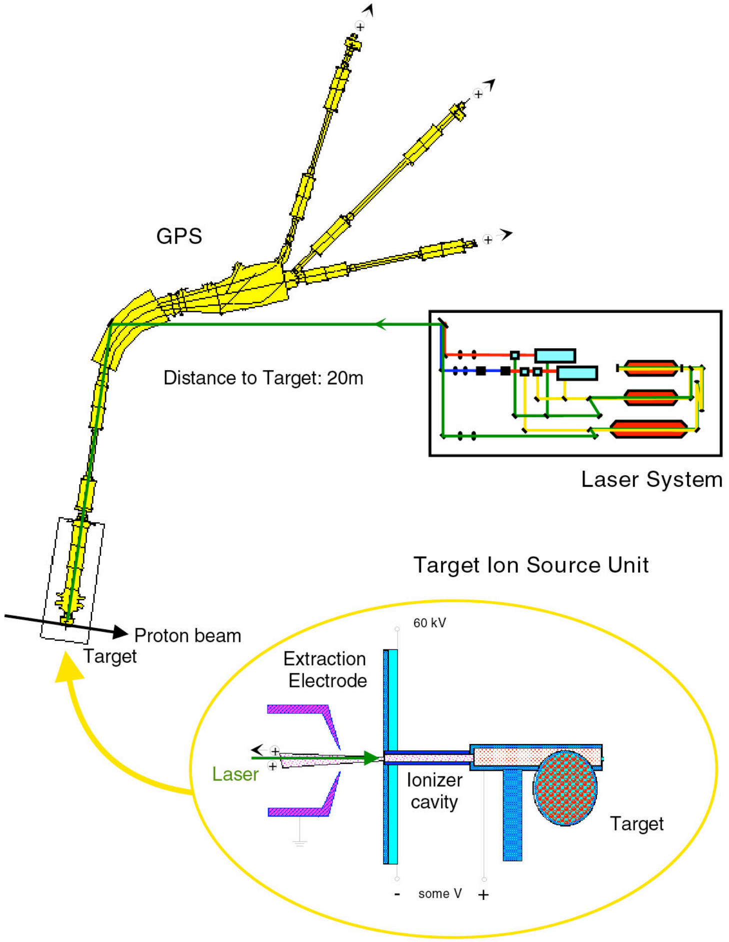

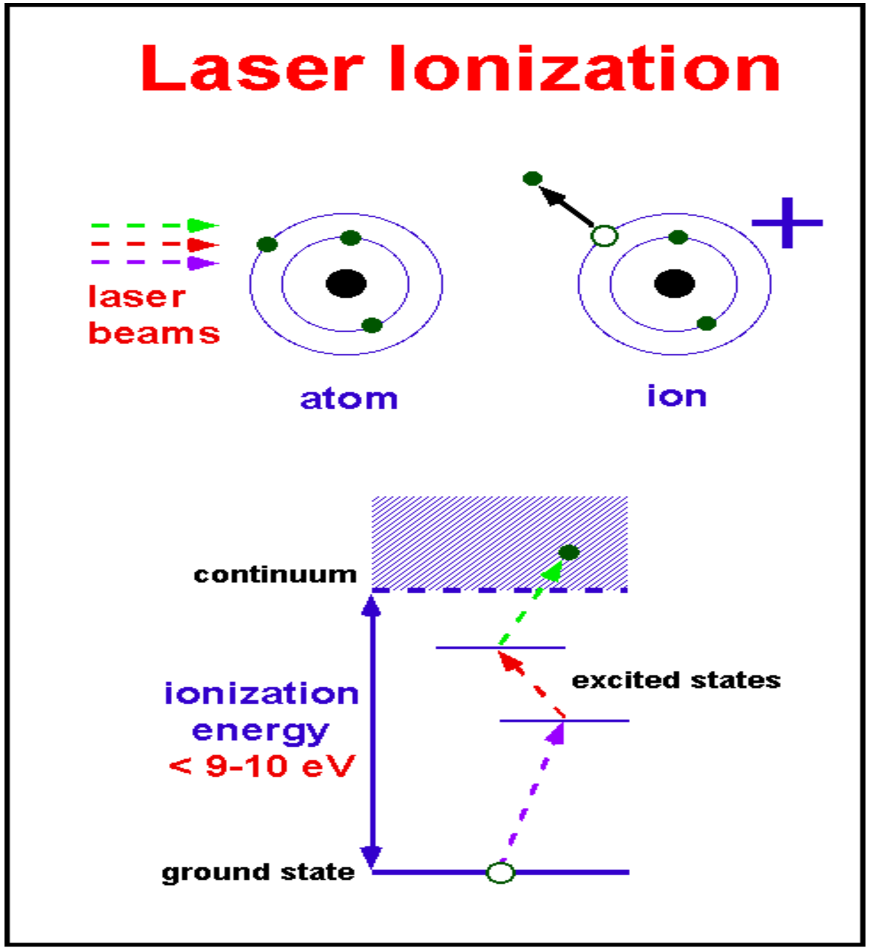

REX-Isolde

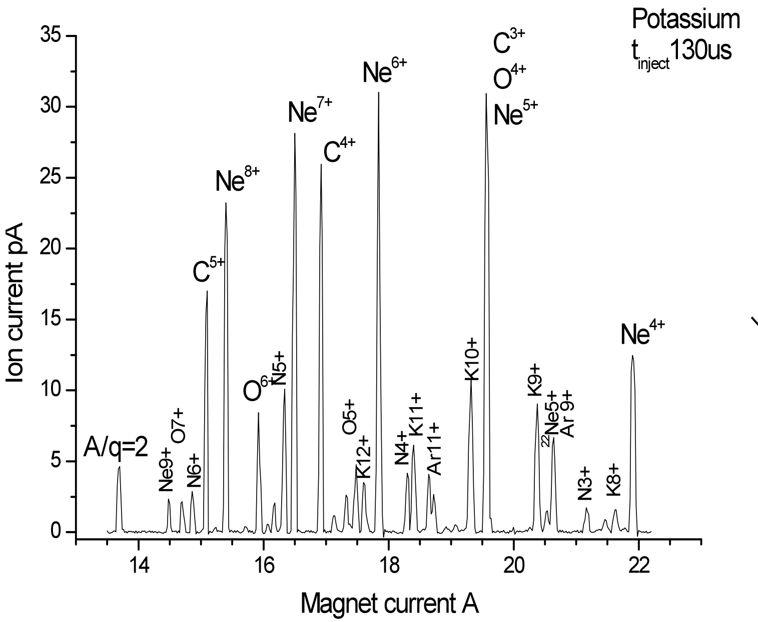

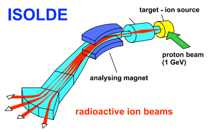

* charge breeding
* 1+ ions to n+

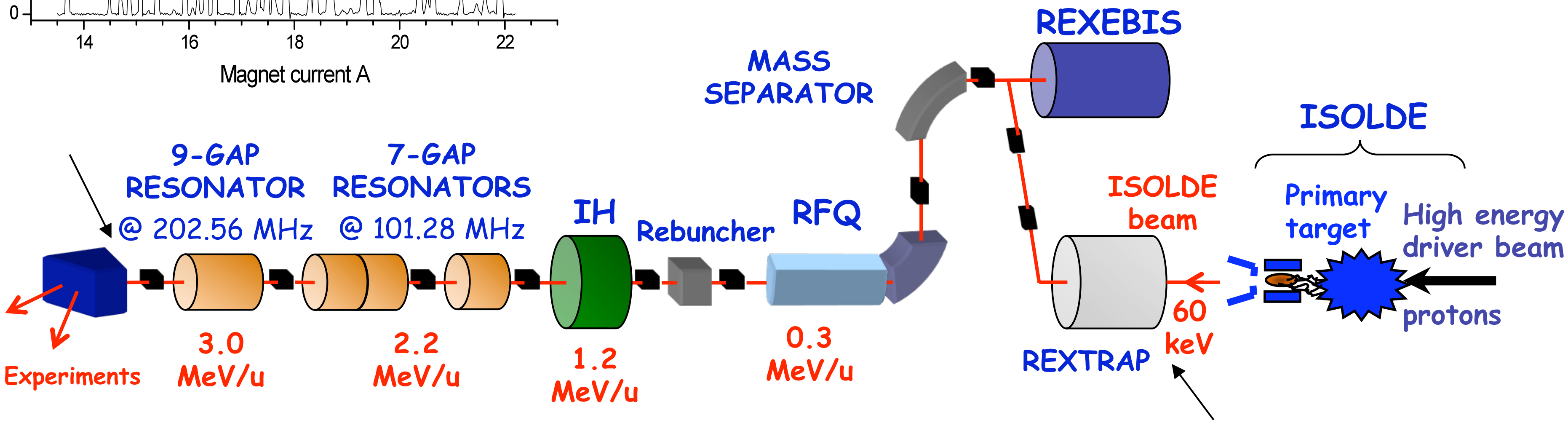

* longitudinal accumulation and bunching
* transverse phase space cooling

* 6 cavities
* 100 and 200 MHz, ~100 kW
* 300 keV/u to 3 MeV/u

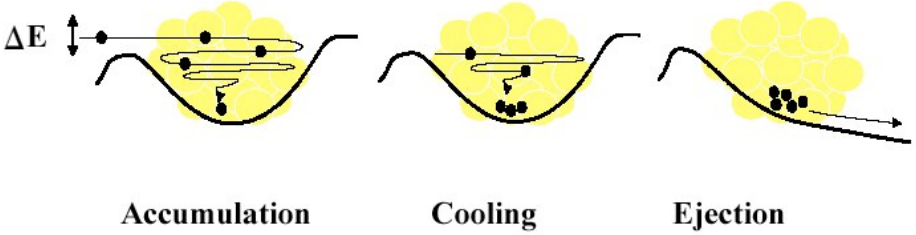

D. Voulot

N=50 and Z=28

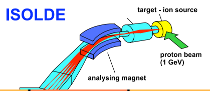

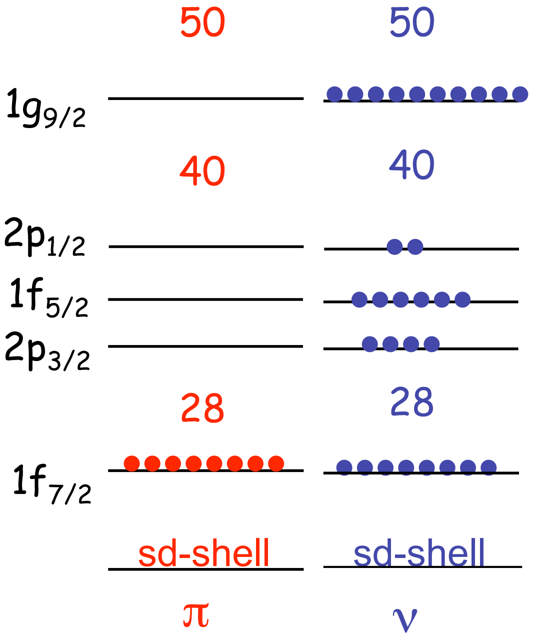

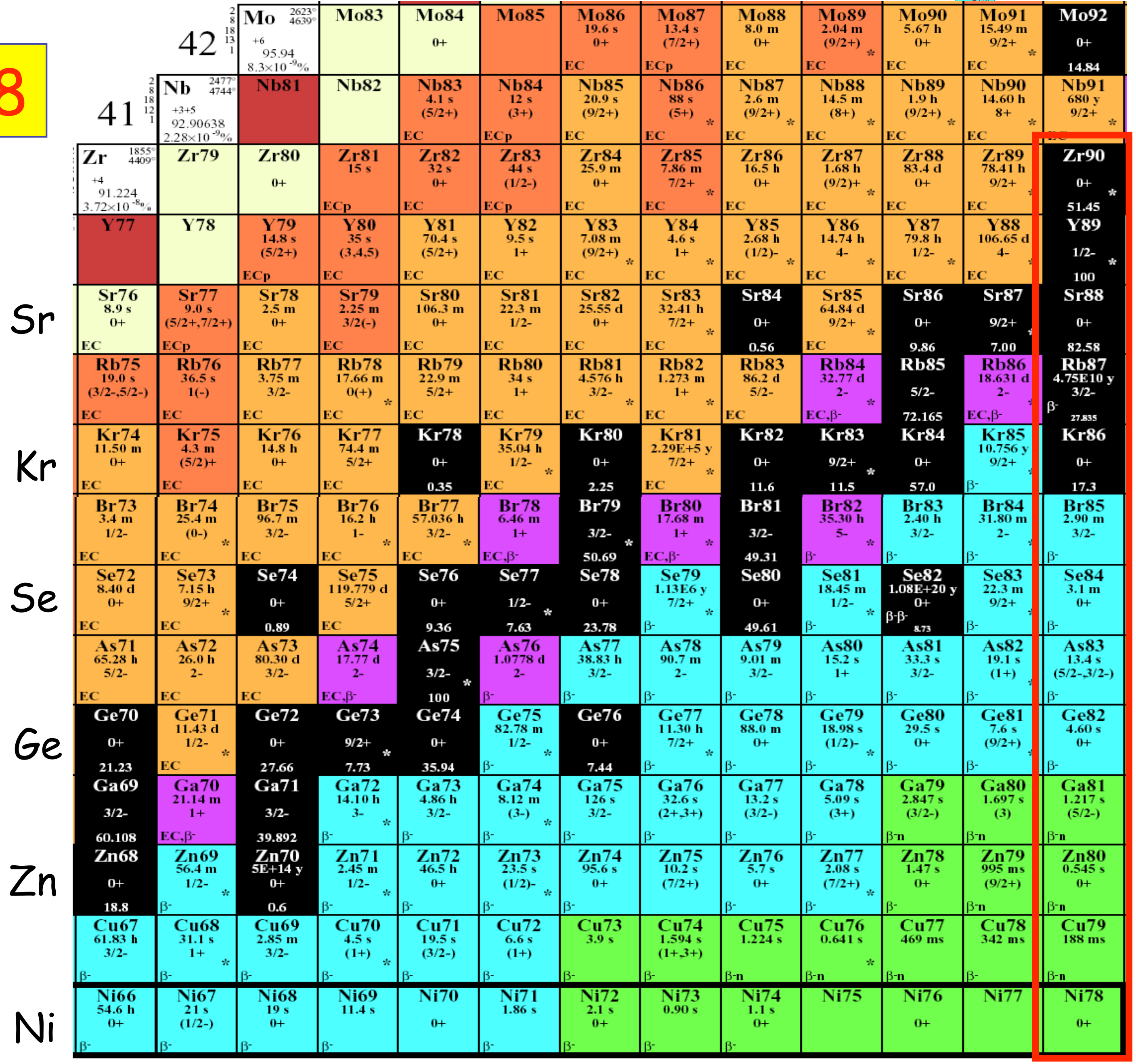

42			Mo 2623° 4639° 2 8 18 13 1 +6 95.94 8.3×10^{-9}%	Mo83	Mo84 0+	Mo85	Mo86 19.6 s 0+ EC	Mo87 13.4 s (7/2+) ECp	Mo88 8.0 m 0+ EC	Mo89 2.04 m (9/2+) * EC	Mo90 5.67 h 0+ EC	Mo91 15.49 m 9/2+ * EC	Mo92 0+ 14.84
41		Nb 2477° 4744° 2 8 18 12 1 +3+5 92.90638 2.28×10^{-9}%	Nb81	Nb82	Nb83 4.1 s (5/2+) EC	Nb84 12 s (3+) ECp	Nb85 20.9 s (9/2+) EC	Nb86 88 s (5+) * EC	Nb87 2.6 m (9/2+) * EC	Nb88 14.5 m (8+) * EC	Nb89 1.9 h (9/2+) * EC	Nb90 14.60 h 8+ * EC	Nb91 680 y 9/2+ *
	Zr 1855° 4409° +4 91.224 3.72×10^{-8}%	Zr79	Zr80 0+	Zr81 15 s ECp	Zr82 32 s 0+ EC	Zr83 44 s (1/2-) ECp	Zr84 25.9 m 0+ EC	Zr85 7.86 m 7/2+ * EC	Zr86 16.5 h 0+ EC	Zr87 1.68 h (9/2)+ * EC	Zr88 83.4 d 0+ EC	Zr89 78.41 h 9/2+ * EC	Zr90 0+ * 51.45
	Y77	Y78	Y79 14.8 s (5/2+) ECp	Y80 35 s (3,4,5) EC	Y81 70.4 s (5/2+) EC	Y82 9.5 s 1+ EC	Y83 7.08 m (9/2+) * EC	Y84 4.6 s 1+ * EC	Y85 2.68 h (1/2)- * EC	Y86 14.74 h 4- * EC	Y87 79.8 h 1/2- * EC	Y88 106.65 d 4- * EC	Y89 1/2- * 100
Sr	Sr76 8.9 s 0+ EC	Sr77 9.0 s (5/2+,7/2+) ECp	Sr78 2.5 m 0+ EC	Sr79 2.25 m 3/2(-) EC	Sr80 106.3 m 0+ EC	Sr81 22.3 m 1/2- EC	Sr82 25.55 d 0+ EC	Sr83 32.41 h 7/2+ * EC	Sr84 0+ 0.56	Sr85 64.84 d 9/2+ * EC	Sr86 0+ 9.86	Sr87 9/2+ * 7.00	Sr88 0+ 82.58
	Rb75 19.0 s (3/2-,5/2-) EC	Rb76 36.5 s 1(-) EC	Rb77 3.75 m 3/2- EC	Rb78 17.66 m 0(+) * EC	Rb79 22.9 m 5/2+ EC	Rb80 34 s 1+ EC	Rb81 4.576 h 3/2- * EC	Rb82 1.273 m 1+ * EC	Rb83 86.2 d 5/2- EC	Rb84 32.77 d 2- * EC,β^-	Rb85 5/2- 72.165	Rb86 18.631 d 2- * EC,β^-	Rb87 4.75E10 y 3/2- β^- 27.835
Kr	Kr74 11.50 m 0+ EC	Kr75 4.3 m (5/2)+ EC	Kr76 14.8 h 0+ EC	Kr77 74.4 m 5/2+ EC	Kr78 0+ 0.35	Kr79 35.04 h 1/2- * EC	Kr80 0+ 2.25	Kr81 2.29E+5 y 7/2+ * EC	Kr82 0+ 11.6	Kr83 9/2+ * 11.5	Kr84 0+ 57.0	Kr85 10.756 y 9/2+ * β^-	Kr86 0+ 17.3
	Br73 3.4 m 1/2- EC	Br74 25.4 m (0-) * EC	Br75 96.7 m 3/2- EC	Br76 16.2 h 1- * EC	Br77 57.036 h 3/2- * EC	Br78 6.46 m 1+ EC,β^-	Br79 3/2- * 50.69	Br80 17.68 m 1+ * EC,β^-	Br81 3/2- 49.31	Br82 35.30 h 5- * β^-	Br83 2.40 h 3/2- β^-	Br84 31.80 m 2- * β^-	Br85 2.90 m 3/2- β^-
Se	Se72 8.40 d 0+ EC	Se73 7.15 h 9/2+ * EC	Se74 0+ 0.89	Se75 119.779 d 5/2+ EC	Se76 0+ 9.36	Se77 1/2- * 7.63	Se78 0+ 23.78	Se79 1.13E6 y 7/2+ * β^-	Se80 0+ 49.61	Se81 18.45 m 1/2- * β^-	Se82 1.08E+20 y 0+ $\beta^-\beta^-$ 8.73	Se83 22.3 m 9/2+ * β^-	Se84 3.1 m 0+ β^-
	As71 65.28 h 5/2- EC	As72 26.0 h 2- EC	As73 80.30 d 3/2- EC	As74 17.77 d 2- EC,β^-	As75 3/2- * 100	As76 1.0778 d 2- β^-	As77 38.83 h 3/2- β^-	As78 90.7 m 2- β^-	As79 9.01 m 3/2- β^-	As80 15.2 s 1+ β^-	As81 33.3 s 3/2- β^-	As82 19.1 s (1+) * β^-	As83 13.4 s (5/2-,3/2-) β^-
Ge	Ge70 0+ 21.23	Ge71 11.43 d 1/2- * EC	Ge72 0+ 27.66	Ge73 9/2+ * 7.73	Ge74 0+ 35.94	Ge75 82.78 m 1/2- * β^-	Ge76 0+ 7.44	Ge77 11.30 h 7/2+ * β^-	Ge78 88.0 m 0+ β^-	Ge79 18.98 s (1/2)- * β^-	Ge80 29.5 s 0+ β^-	Ge81 7.6 s (9/2+) * β^-	Ge82 4.60 s 0+ β^-
	Ga69 3/2- 60.108	Ga70 21.14 m 1+ EC,β^-	Ga71 3/2- 39.892	Ga72 14.10 h 3- * β^-	Ga73 4.86 h 3/2- β^-	Ga74 8.12 m (3-) * β^-	Ga75 126 s 3/2- β^-	Ga76 32.6 s (2+,3+) β^-	Ga77 13.2 s (3/2-) β^-	Ga78 5.09 s (3+) β^-	Ga79 2.847 s (3/2-) β^-n	Ga80 1.697 s (3) β^-n	Ga81 1.217 s (5/2-) β^-n
Zn	Zn68 0+ 18.8	Zn69 56.4 m 1/2- * β^-	Zn70 5E+14 y 0+ 0.6	Zn71 2.45 m 1/2- * β^-	Zn72 46.5 h 0+ β^-	Zn73 23.5 s (1/2)- * β^-	Zn74 95.6 s 0+ β^-	Zn75 10.2 s (7/2+)	Zn76 5.7 s 0+ β^-	Zn77 2.08 s (7/2+) * β^-	Zn78 1.47 s 0+ β^-	Zn79 995 ms (9/2+) β^-n	Zn80 0.545 s 0+ β^-n
	Cu67 61.83 h 3/2- β^-	Cu68 31.1 s 1+ * β^-	Cu69 2.85 m 3/2- β^-	Cu70 4.5 s (1+) * β^-	Cu71 19.5 s (3/2-) β^-	Cu72 6.6 s (1+) β^-	Cu73 3.9 s β^-	Cu74 1.594 s (1+,3+) β^-	Cu75 1.224 s β^-n	Cu76 0.641 s * β^-n	Cu77 469 ms β^-n	Cu78 342 ms β^-	Cu79 188 ms β^-n
Ni	Ni66 54.6 h 0+ β^-	Ni67 21 s (1/2-) β^-	Ni68 19 s 0+ β^-	Ni69 11.4 s β^-	Ni70 0+	Ni71 1.86 s β^-	Ni72 2.1 s 0+ β^-	Ni73 0.90 s β^-	Ni74 1.1 s 0+ β^-	Ni75	Ni76 0+	Ni77	Ni78 0+

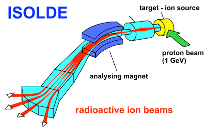

• “Safe” Coulomb Excitation experiments

- ➢ particle (CD) - γ correlations

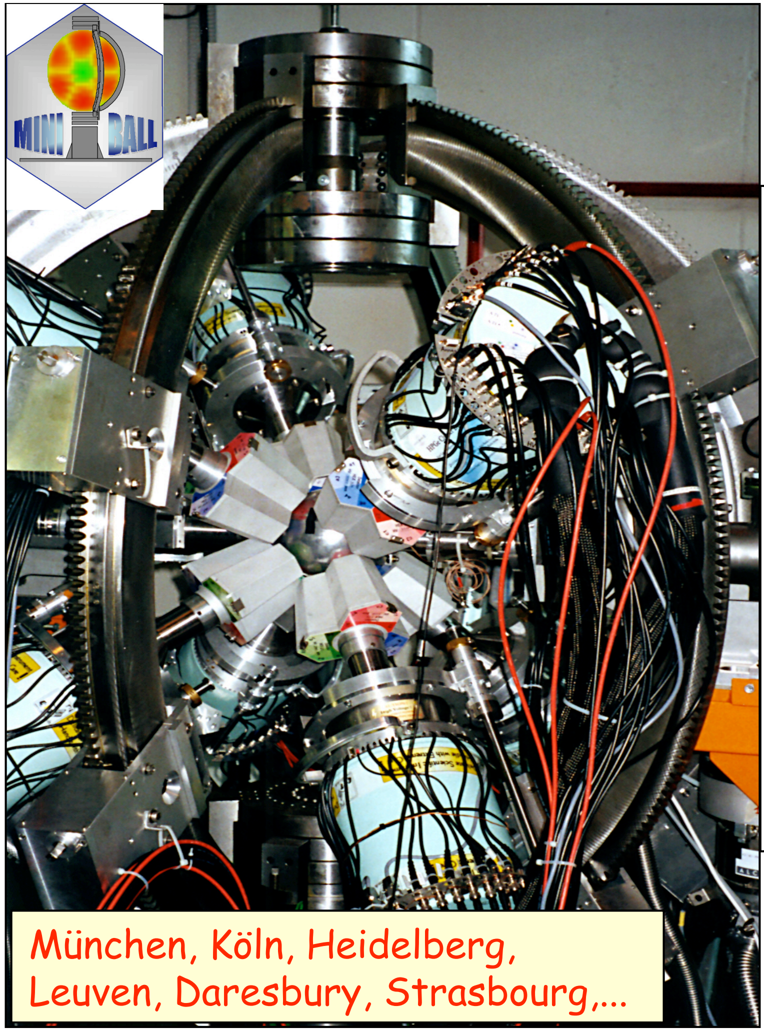

München, Köln, Heidelberg,
Leuven, Daresbury, Strasbourg,...

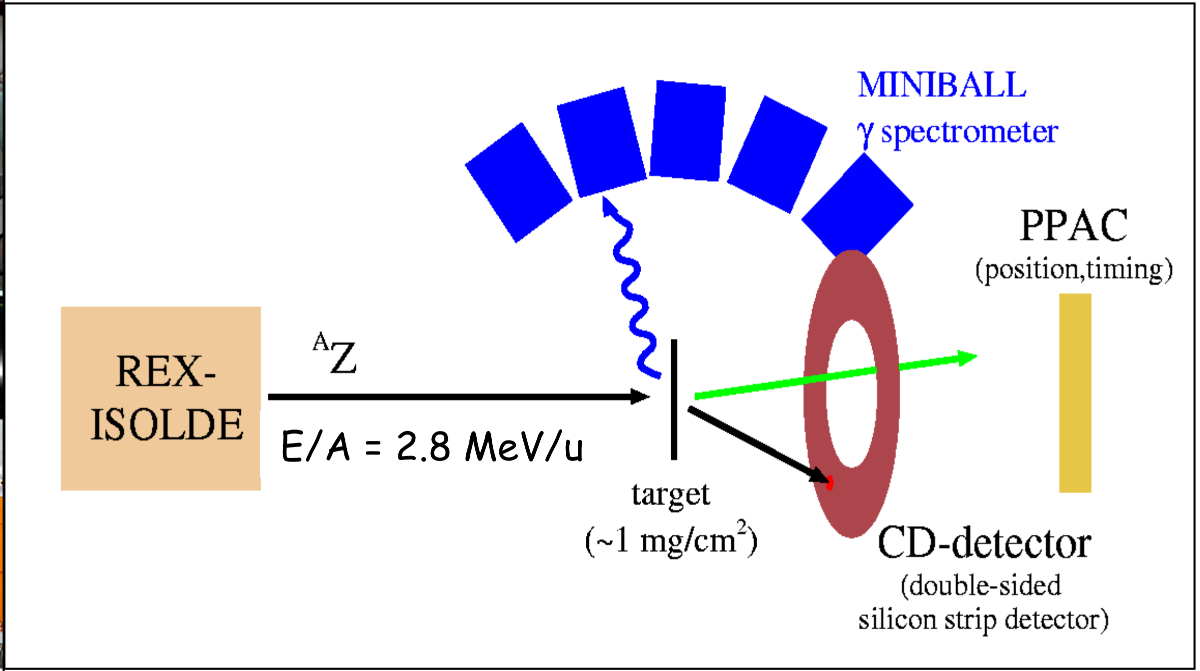

2006

$^{80}Zn_{50}$

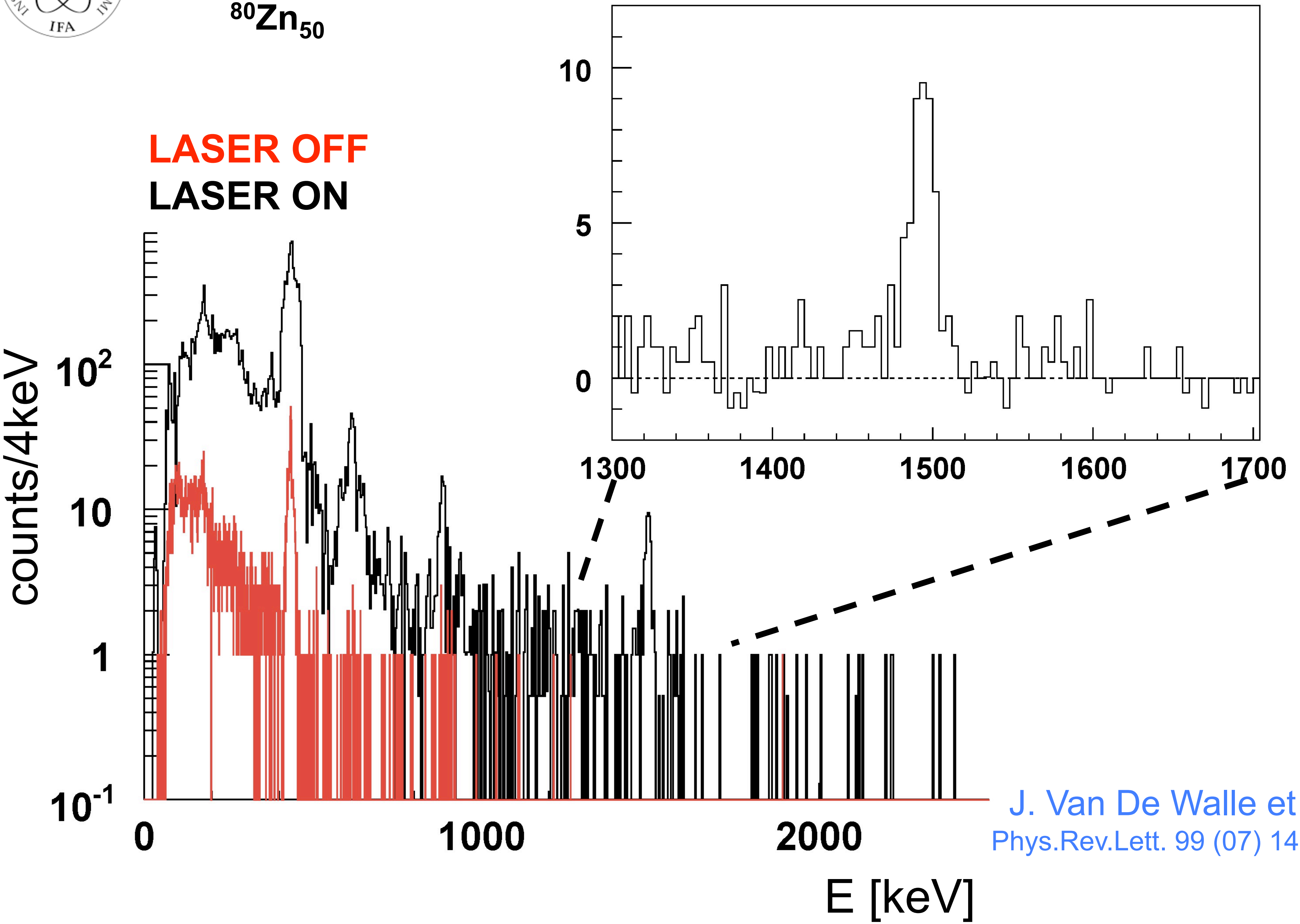

J. Van De Walle et al,
Phys.Rev.Lett. 99 (07) 142501

-2 major shell closures
-Neutron Rich Nuclei
-Even-Even Isotopes

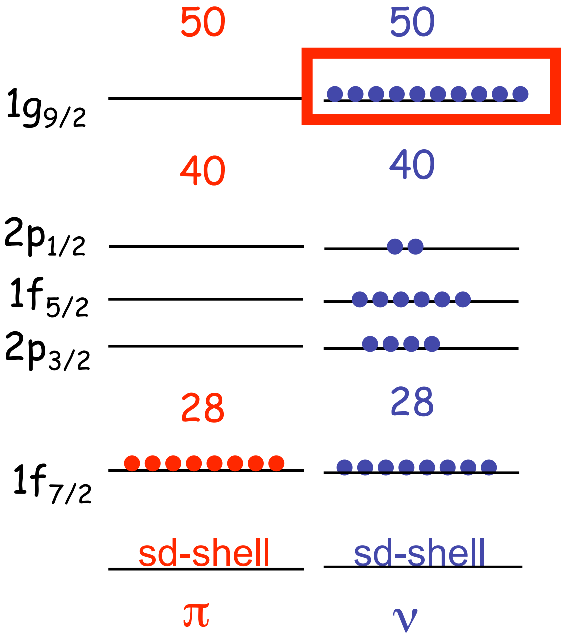

^{78}Ni

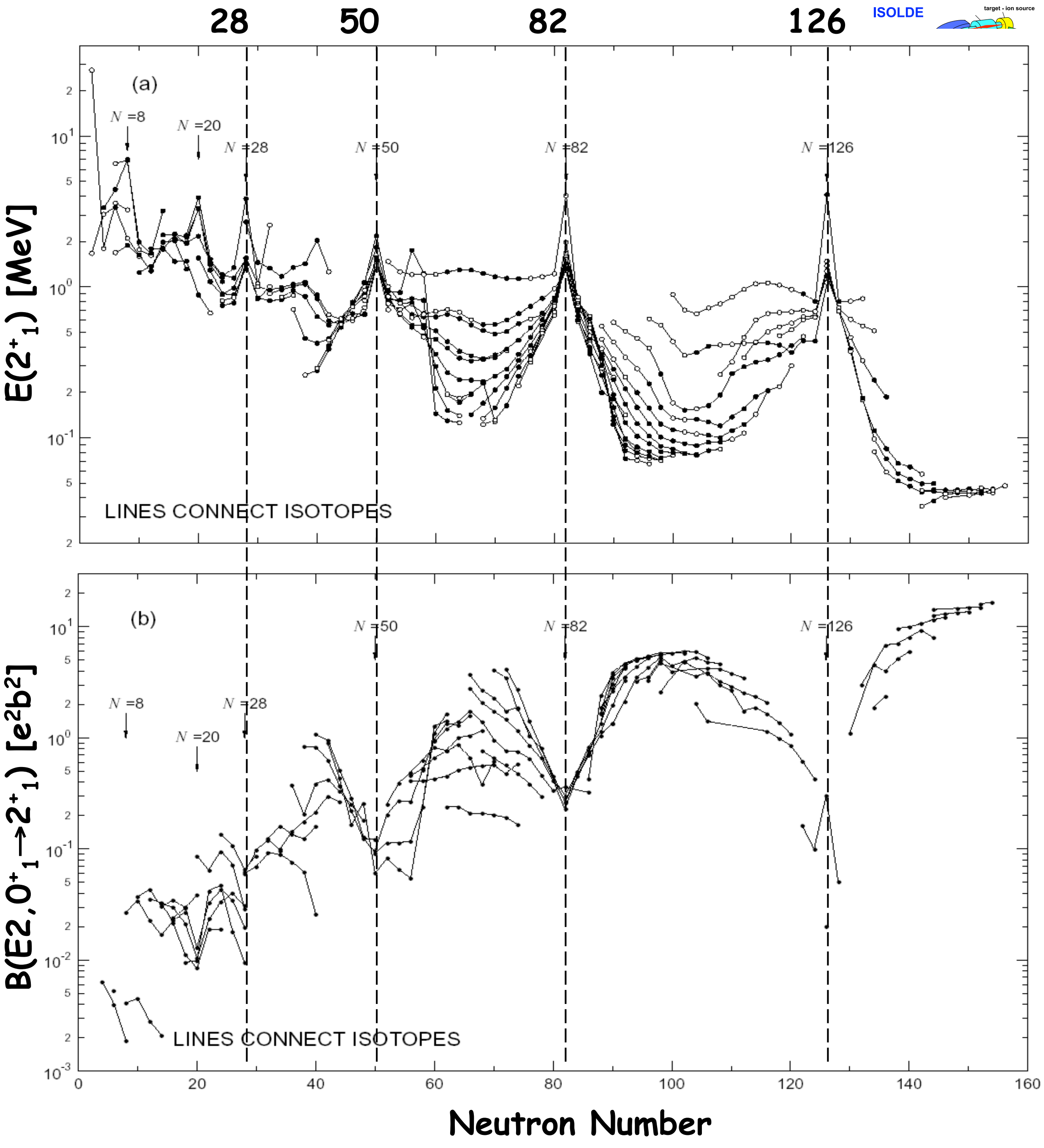

J. Van De Walle

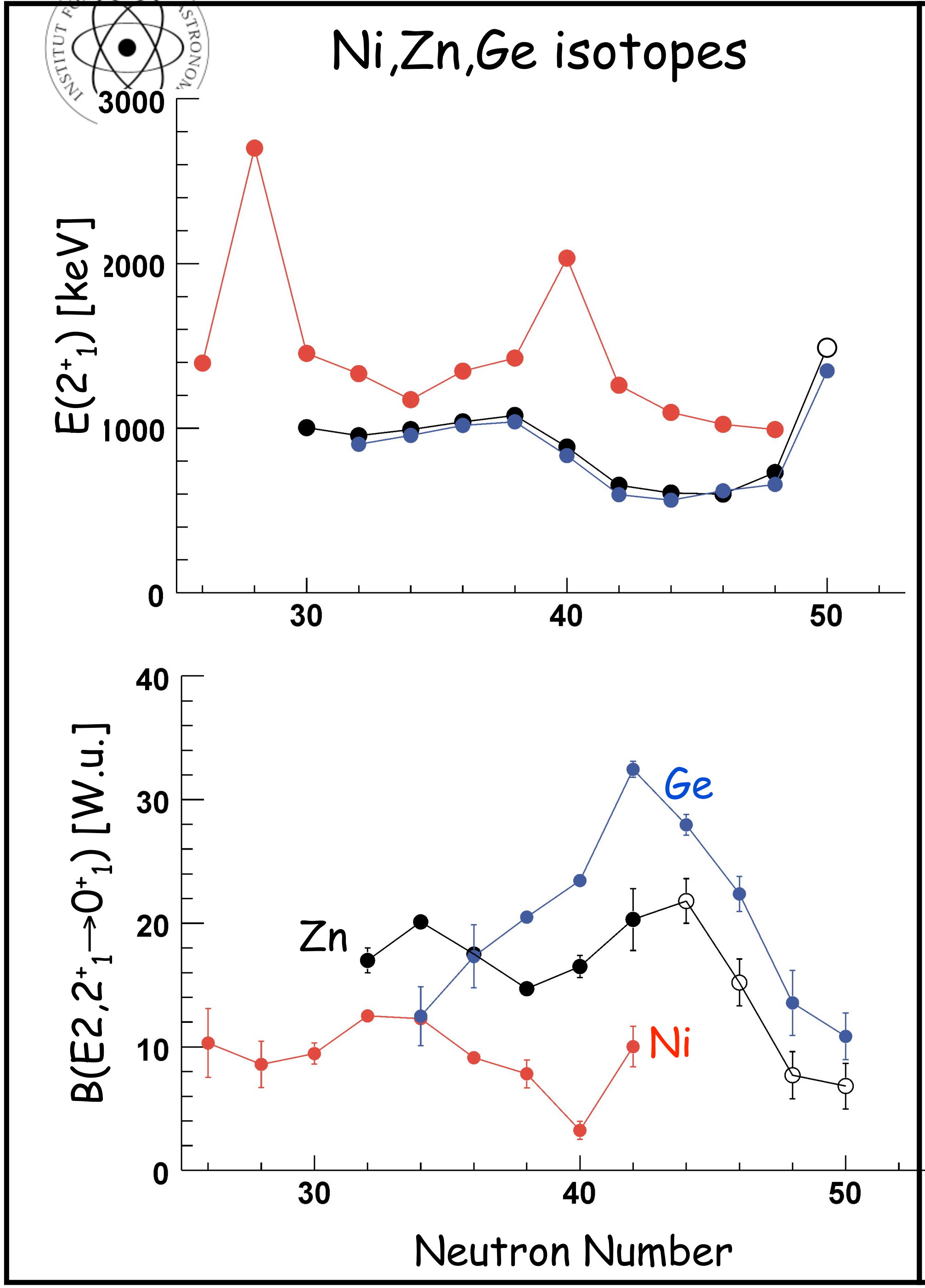

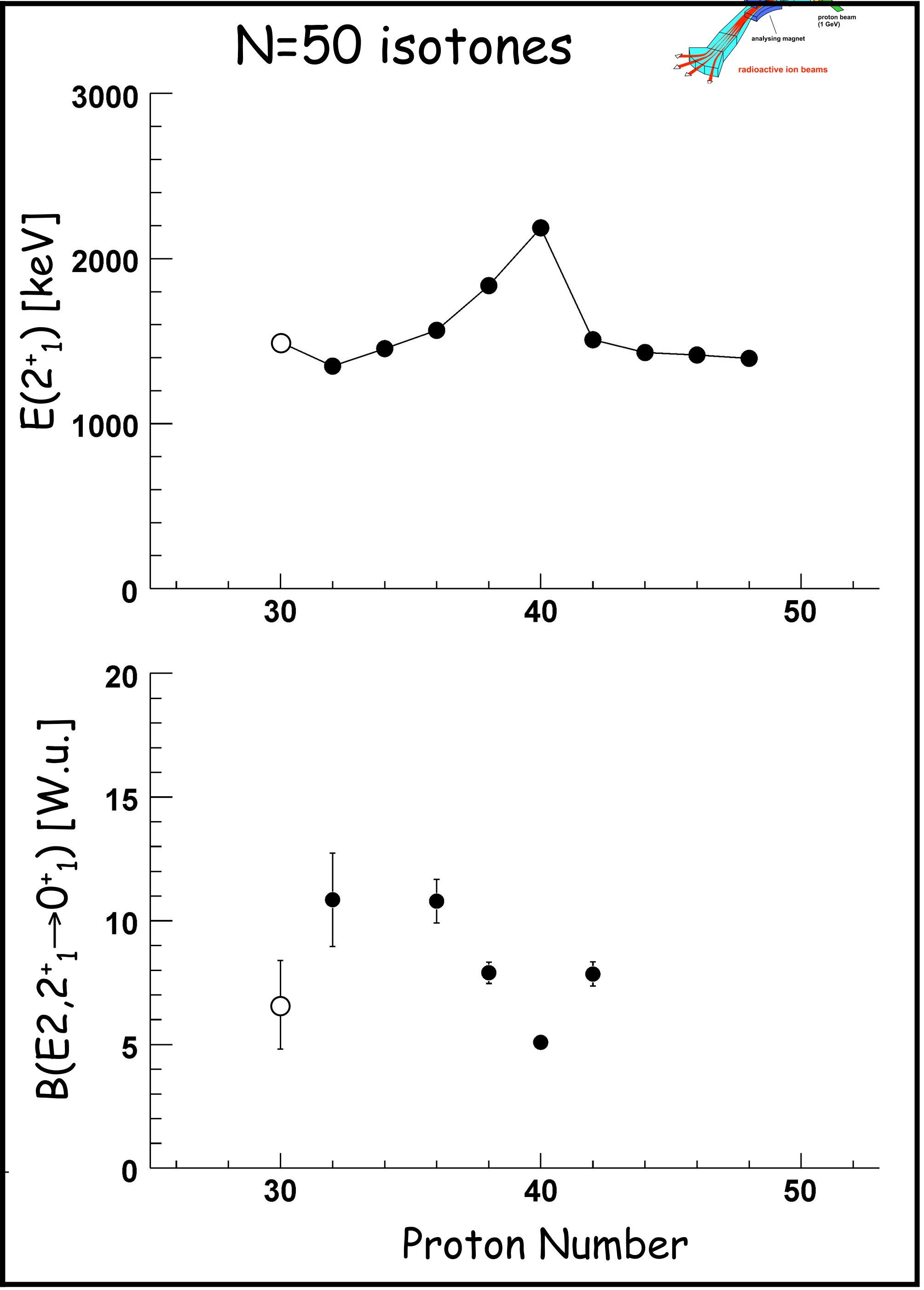

Nuclear halo states

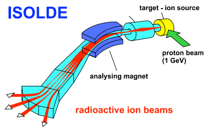

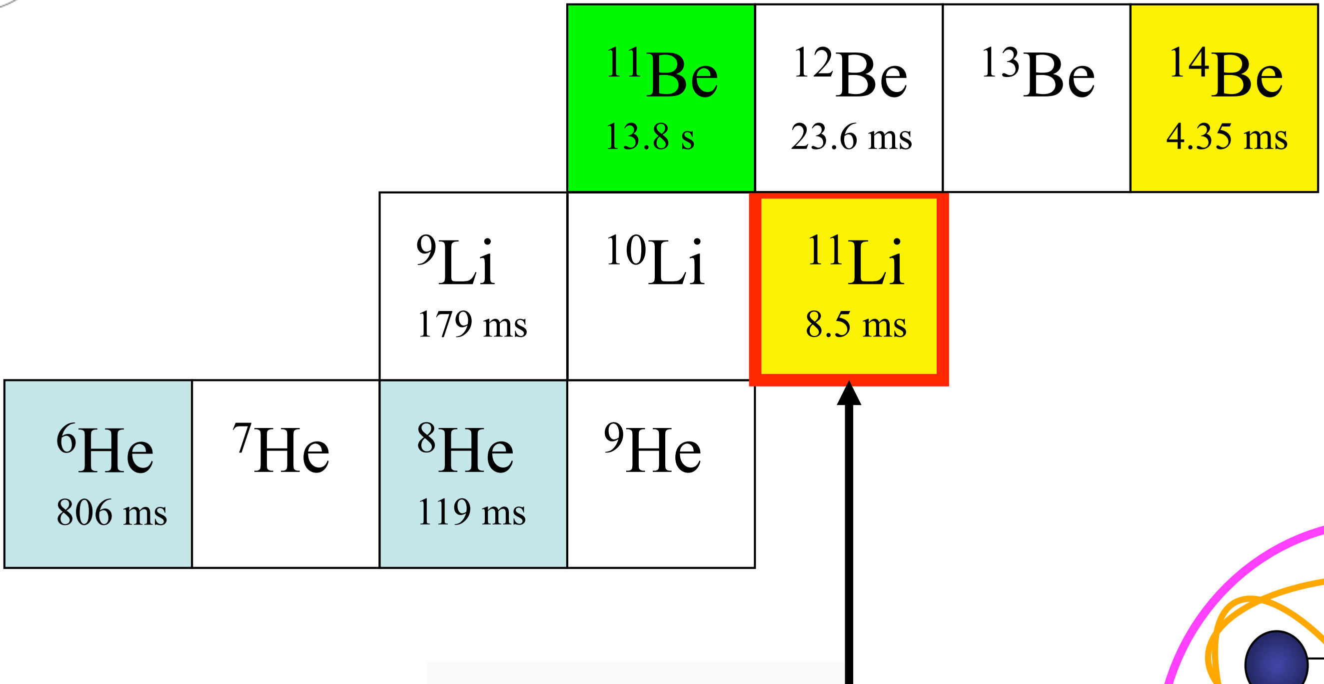

			^{11}Be 13.8 s	^{12}Be 23.6 ms	^{13}Be	^{14}Be 4.35 ms
		^{9}Li 179 ms	^{10}Li	^{11}Li 8.5 ms		
^{6}He 806 ms	^{7}He	^{8}He 119 ms	^{9}He			

N=8

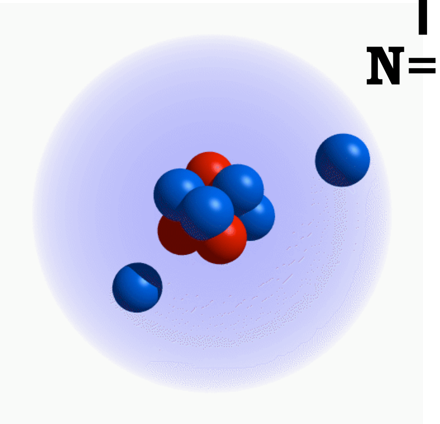

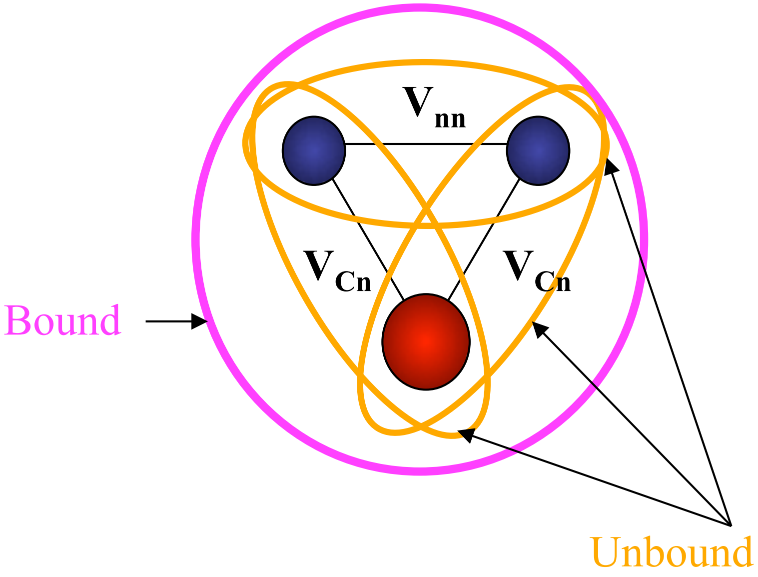

B. Jonson

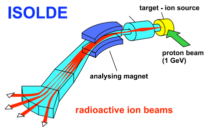

^{9}Li+^{2}H→t+^{8}Li*

Eksempel på neutron transfer fra ^{9}Li til deuteron – danner en triton

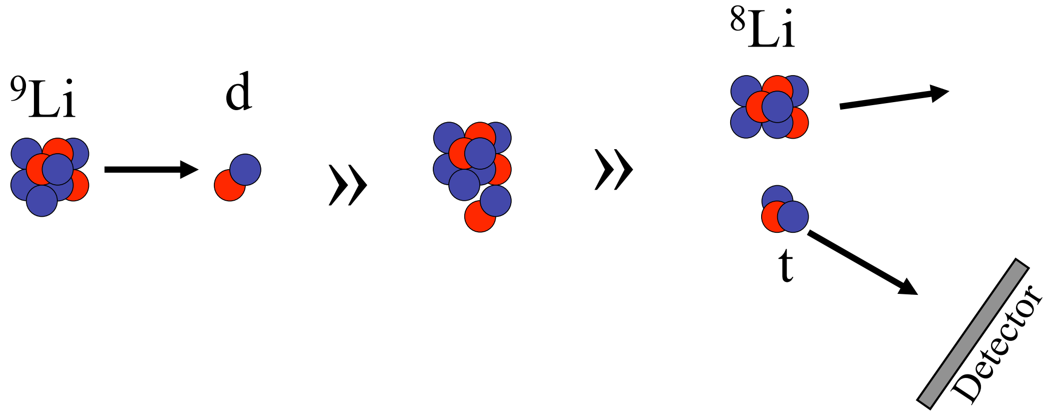

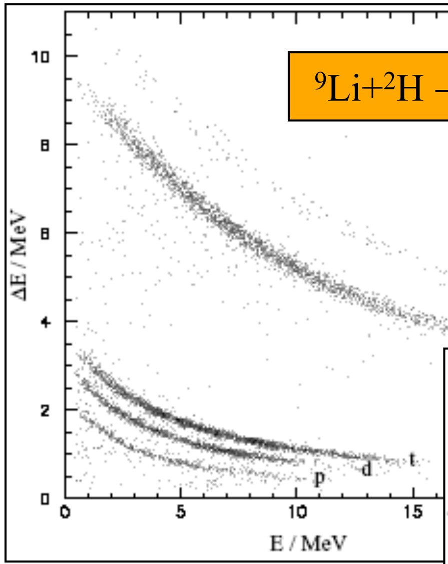

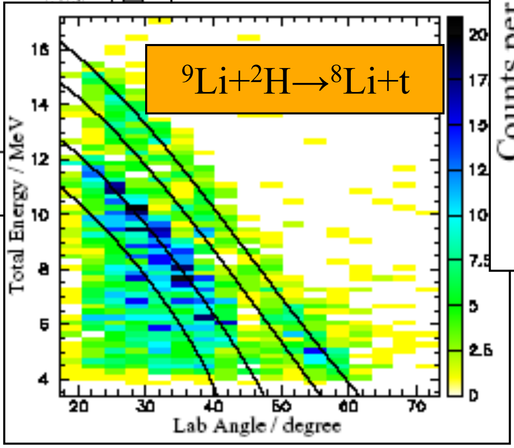

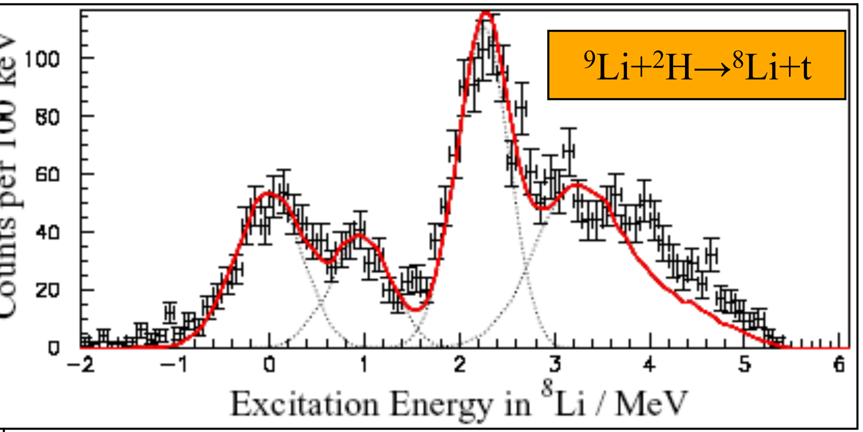

H.B.Jeppesen *et al.* Nucl. phys. **A748** (2005) 374

H.B.Jeppesen *et al.* Phys. Lett. **B635** (2006) 17

H.B. Jeppesen

Proton knock-out, ^{12}Be

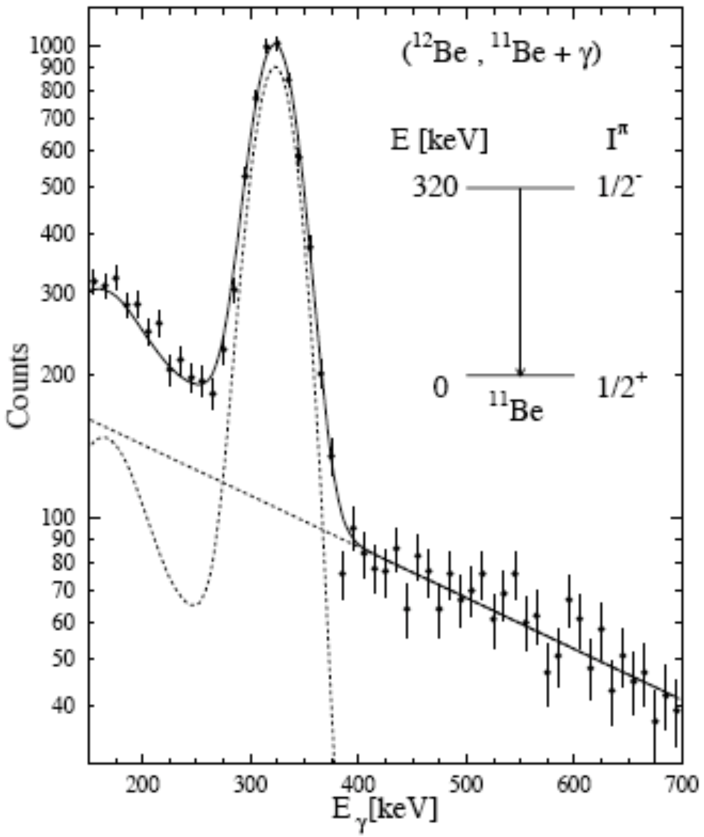

FIG. 1. Measured gamma-ray spectrum in the projectile rest frame in coincidence with ^{11}Be residues. The full-drawn line is the result of a fit using a simulated line shape of the 320 keV gamma ray and an exponential background, both shown as dashed lines.

NSCL/MSU (in-flight beam):

Fjerner proton pludseligt fra ^{12}Be

Befolker både s- og p-tilstande i ^{11}Be

Cirka lige meget s og p i ^{12}Be g.s.

A. Navin et al, Phys.Rev.Lett. 85 (2000) 266

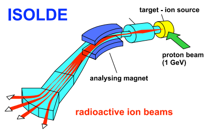

^{24}O dobbelt magisk !

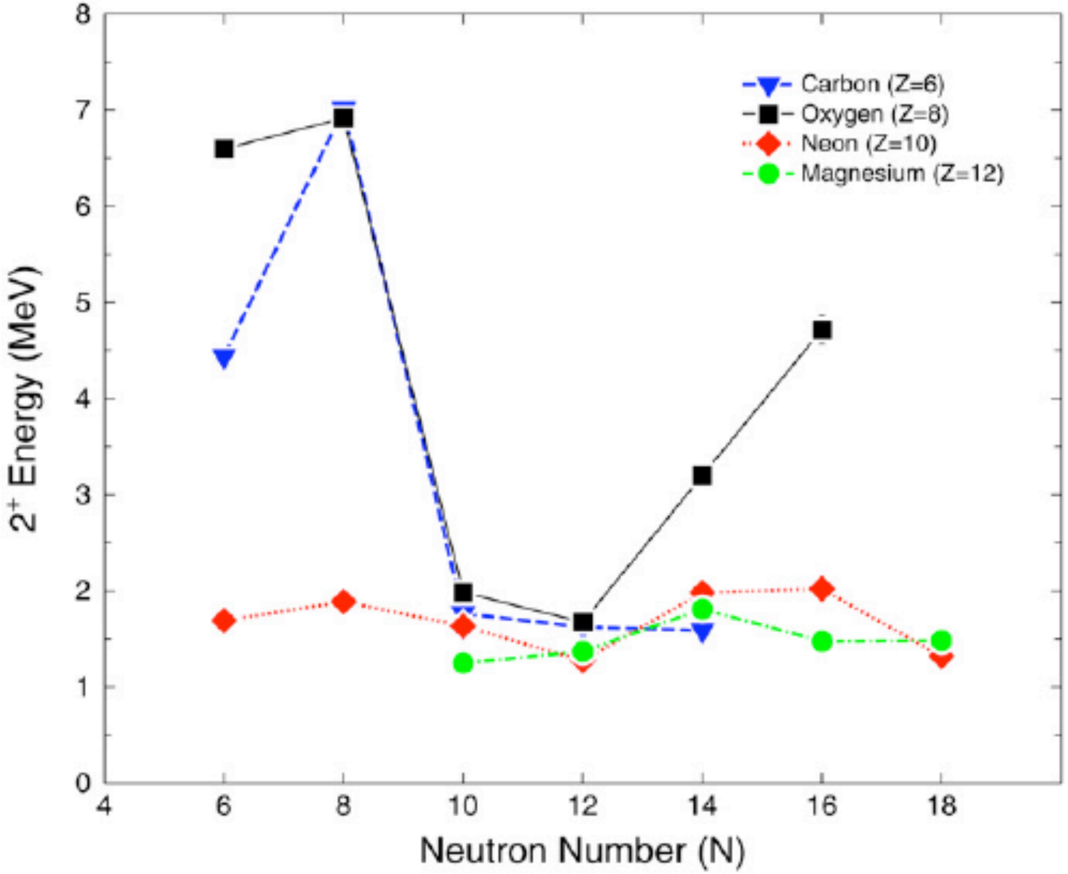

Fig. 4. The experimental 2_1^+ energies for the even–even isotopes of oxygen ($Z = 8$), including the present result at $N = 16$, are shown by the black squares with their errors. Also shown are the experimental 2_1^+ energies for carbon ($Z = 6$) (upside-down triangle, blue), neon ($Z = 10$) (diamond, red) and magnesium ($Z = 12$) (circle, green) [21,22]. Clearly noticed is the increase in the 2_1^+ energy for ^{24}O relative to the nearby even–even nuclei indicating the large $N = 16$ shell gap for $Z = 8$. (For

NSCL/MSU (in-flight beam):

Fragmentation af ^{26}F beam

Ser på neutron-^{23}O koincidenser (ingen bundne tilstande i ^{24}O)

Den “klassiske” dobbelt magiske kerne ^{28}O er ubundet

C.R. Hoffman et al,
Phys.Lett. B672 (2009) 17

AU / ISOLDE gruppen:

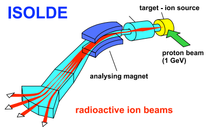

- Karsten Riisager
- Hans Fynbo

- Solveig Hyldegaard, PhD studerende
- Oliver Kirsebom, PhD studerende
- Jacob Johansen, PhD studerende

- + grupper i Madrid, Göteborg, CERN, …